

# Overoxidized poly(3,4-ethylenedioxythiophene)-overoxidized polypyrrole composite films with enhanced electrocatalytic ability for rutin and luteolin determination

Rongqian Meng<sup>1,2</sup>, Jianke Tang<sup>1,2</sup>, Hong Yang<sup>1,2</sup>, Lijun Guo<sup>1</sup>, Yongbo Song<sup>1</sup>,  
Qiaoling Li (✉)<sup>3</sup>, Yulan Niu (✉)<sup>1</sup>

<sup>1</sup> Department of Chemistry and Chemical Engineering, Taiyuan Institute of Technology, Taiyuan 030008, China

<sup>2</sup> School of Chemical Engineering and Technology, North University of China, Taiyuan 030051, China

<sup>3</sup> School of Science, North University of China, Taiyuan 030051, China

© Higher Education Press 2023

**Abstract** In this study, a simple and effective method was proposed to improve the electrocatalytic ability of overoxidized poly(3,4-ethylenedioxythiophene)-overoxidized polypyrrole composite films modified on glassy carbon electrode for rutin and luteolin determination. The composite electrode was prepared by cyclic voltammetry copolymerization with LiClO<sub>4</sub>-water as the supporting electrolyte. The peak current of rutin and luteolin on the composite electrode gradually decreased or even disappeared with the increase in the positive potential limit. After incubation in NaOH-ethanol solution with a volume ratio of 1:1, the composite electrodes prepared at positive potential limit greater than 1.5 V exhibited enhanced differential pulse voltammetry peak currents, reduced charge transfer resistance, larger effective specific surface area and higher electron transfer rate constant. The composite electrode prepared in the potential range of 0–1.7 V showed optimal electrocatalytic performance. The X-ray photoelectron spectroscopy results indicated that the content of –SO<sub>2</sub>/–SO and –C=N– groups in the composite film increased significantly after incubation. Further, the Raman spectra and Fourier transform infrared spectra revealed that the thiophene ring structure changed from benzene-type to quinone-type, and the quinone-type pyrrole ring was formed. The electrocatalytic mechanism of the composite film was proposed based on the experimental results and further verified by Density Functional Theory calculation.

**Keywords** overoxidized poly(3, 4-ethylenedioxythiophene)-overoxidized polypyrrole, rutin, luteolin, incubation, electrocatalytic mechanism

## 1 Introduction

Poly(3,4-ethylenedioxythiophene) (PEDOT) and polypyrrole (PPy) as widely used conductive polymers, had the advantages of high electrical conductivity, good film formation, narrow energy gap width, good biocompatibility, etc. [1–3]. The two had some common features, such as five-membered heterocyclic ring in structure, cationic radical polymerization mechanism, anionic dopant type, polymerization potential range matching, solubility in water [4–6]. However, both are susceptible to be overoxidized under certain conditions, such as exposure to strong oxidants and high positive potential [7,8]. In 1982, Bull et al. [9] found that when the polymerization potential was greater than 0.6 V, irreversible overoxidation occurred in PPy. When the polymerization potential was greater than 0.8 V, PEDOT began to overoxidation, but the degree of overoxidation was small. When the polymerization potential was greater than 1.2 V, overoxidation could not be ignored [10]. Both the polymers had similar overoxidation mechanism, i.e., by the nucleophilic attack of HO·, OH<sup>–</sup>, and O<sub>2</sub><sup>–</sup> [7,11–13], the –C=O and –SO<sub>2</sub>/–SO groups was formed on the ethylenedioxy group and thiophene ring of EDOT, and –C=O group was formed on the β-position C of the pyrrole ring, resulting in a shorter polymer conjugation chain and a decrease in the electroactivity [7,8,12,13]. However, the created oxygen-containing groups endowed the overoxidized polymer with new properties, such as electronegativity, and selective permeability [12,14,15]. Several studies showed that the overoxidized poly(3,4-ethylenedioxythiophene) (oPEDOT) showed relatively better conductivity [16,17] but inferior selectivity than the overoxidized polypyrrole (oPPy) [18]. Therefore, the

Received July 24, 2022; accepted September 17, 2022

E-mails: qiaolingl@163.com (Li Q.), Niuyul@tit.edu.cn (Niu Y.)

combination of oPEDOT and oPPy was expected to provide complementary advantages, thereby enhancing the electrochemical performance.

The detection sensitivity of responsive molecules was an important aspect to evaluate the electrocatalytic performance of electrode materials [19]. Rutin and luteolin, as common flavonoids, were widely found in a variety of plants, seeds, and flowers, such as *Flos Sophorae Immaturus* and *Forsythia suspensa* [20], and had a wide range of pharmacological properties, such as anti-tumor, anti-inflammatory, and antibacterial effects [21]. Both of them all contain ortho-diphenol groups in their structures, which were easily oxidized on the surface of active electrodes. So it was feasible to investigate the electrocatalytic activity of the prepared electrodes by detecting the oxidized currents of rutin and luteolin [22,23].

In this study, oPEDOT-oPPy composite films modified on glassy carbon electrode (oPEDOT-oPPy/GCE) was prepared by cyclic voltammetry (CV) copolymerization and subsequent incubation, which showed good electrocatalytic activity for rutin and luteolin. The electrochemical performance of this electrode material was investigated by differential pulse voltammetry (DPV) peak current, charge transfer resistant, effective specific surface area and electron transfer rate constant. X-ray photoelectron spectroscopy (XPS), Raman spectroscopy and Fourier transform infrared spectra (FTIR) were used to analyze the structural changes in the oPEDOT-oPPy/GCE before and after incubation. Density functional theory (DFT) calculation was performed to investigate the energy gap ( $E_g$ ) between the highest occupied molecular orbital (HOMO) and lowest unoccupied molecular orbital (LUMO) of oPEDOT and oPPy oligomers and the adsorption energy of these oligomers with luteolin. Finally, the mechanism of the enhanced electrocatalytic ability of oPEDOT-oPPy composite films after incubation was proposed based on the experimental and verified by DFT calculation.

## 2 Experimental

### 2.1 Materials

Rutin (95%), luteolin (95%), EDOT (99%) and pyrrole (98%) were obtained from Aladdin Biochemical Technology Co., Ltd. (Shanghai, China).  $\text{Na}_2\text{HPO}_4$  (99.0%),  $\text{NaH}_2\text{PO}_4$  (99.0%), absolute methanol (99.7%),  $\text{LiClO}_4$  (99%), acetic acid (99.5%) and sodium acetate (99.0%) were purchased from Sinopharm Chemical Reagent Co. Ltd. (Shanghai, China). The stock solution of rutin was prepared with methanol and stored in a refrigerator at 4 °C. Acetate buffer solution (ABS, 0.1 mol·L<sup>-1</sup>) prepared with acetic acid and sodium acetate was employed as test solvent. Unless stated otherwise, other reagents used were

analytical grade. All the solutions were prepared with deionized water.

### 2.2 Equipment

All the electrochemical experiments including CV, DPV, electrochemical impedance spectroscopy (EIS) and chronocoulometry (CC) were performed on an electrochemical workstation (CHI660E, Shanghai CH Instrument, China). A conventional three-electrode system was employed. The working electrode was GCE (diameter: 3 mm), the auxiliary and reference electrodes were a Pt foil and a saturated calomel electrode (SCE), respectively. SEM images were obtained by using a JSM-7200F scanning electron microscope (JEOL, Japan). XPS were obtained by Escalab 250Xi XPS spectrometer (Thermo Fisher Scientific, USA). The FTIR spectra were measured by an FTIR-8400S spectrometer (Shimadzu, Japan). The Raman spectra were measured by LabRAM HR Evolution spectrometer (Horiba, France). All experiments were carried out at room temperature.

### 2.3 Electrochemical measurement

Before the electropolymerization, the bare GCE was polished with 0.3, 0.05 μm alumina powder in turn, then it was separately rinsed with ethanol and water, and dried. The treated electrode was placed in a solution of 0.1 mol·L<sup>-1</sup>  $\text{KNO}_3$  containing 5 mmol·L<sup>-1</sup>  $\text{K}_3[\text{Fe}(\text{CN})_6]$ / $\text{K}_4[\text{Fe}(\text{CN})_6]$  for CV scanning (potential range from -0.1 to +0.5 V, scan rate: 50 mV·s<sup>-1</sup>), until the stable peak difference was about 80 mV.

PEDOT-PPy/GCE was prepared in the aqueous solution containing 4 mmol·L<sup>-1</sup> EDOT, 2 mmol·L<sup>-1</sup> pyrrole and 0.03 mol·L<sup>-1</sup>  $\text{LiClO}_4$  by CV polymerization method with a scan rate of 0.08 V·s<sup>-1</sup> and a cycle number of 2, and the potential polymerization ranges were set as 0–0.8, 0–1.0, 0–1.5, 0–1.7 and 0–1.9 V, respectively. Then the constructed electrode was incubated in 20 mL of NaOH-ethanol solution with a volume ratio of 1:1 for 30 min for rutin and luteolin determination.

DPV measurements were recorded in the potential window between 0 and 0.8 V with a pulse amplitude of 0.05 V, a pulse width of 0.05 s, a step potential of 0.005 V and a pulse period 0.5 s. The EIS experiment was performed in a 0.1 mol·L<sup>-1</sup> KCl containing 5.0 mmol·L<sup>-1</sup>  $[\text{Fe}(\text{CN})_6]^{3-/4-}$  solution (frequency range: 100 mHz–100 kHz, AC amplitude: 10 mV). The CC experiment was carried out in 0.1 mol·L<sup>-1</sup> KCl containing 1.0 mmol·L<sup>-1</sup>  $\text{K}_3[\text{Fe}(\text{CN})_6]$ , with a potential range of 0.2–0.6 V.

### 2.4 Computational method

The DFT calculations were performed using the Gaussian 09 program package. For the convenience of calculation, the hexamer structure (oPEDOT<sub>6</sub> and oPPy<sub>6</sub>) was

selected as the calculation object [24], which could reflect the structural changes in the oPEDOT-oPPy polymerization chain before and after incubation. The geometric optimization of different molecules, including (a) oPEDOT<sub>6</sub> and (b) oPPy<sub>6</sub> before incubation, (c) oPEDOT<sub>6</sub> and (d) oPPy<sub>6</sub> after incubation, and (e) the complex of these molecules with luteolin, was performed to locate all the stationary points using the B3LYP-D3/6-311+G(d, p) basis set. Natural bond orbital analysis was used to obtain further insight into the electronic properties of all the optimized structures. Further, the HOMO and LUMO distribution of these structures were obtained by Multiwfn program. The  $E_g$  value of HOMO-LUMO was calculated to evaluate the conductivity of oPEDOT-oPPy composite films.

The adsorption energy ( $\Delta E_{ad}$ ) of luteolin (e) on the a, b, c, and d molecules was determined using the following Eq. (1):

$$\Delta E_{ad} = E_{\text{complex}} - E_{\text{adsorbent}} - E_e, \quad (1)$$

where the adsorbent is a, b, c, or d.  $E_{\text{complex}}$  is the energy

of adsorbent/luteolin complex (a/e, b/e, c/e, or d/e),  $E_{\text{adsorbent}}$  is the energy of adsorbent molecule, and  $E_e$  is the energy of luteolin. The  $\Delta E_{ad}$  was calculated to assess the adsorption ability of the oPEDOT-oPPy composite films [25].

### 3 Results and discussion

#### 3.1 Electrochemical characterization

##### 3.1.1 CV polymerization behavior

The influence of electropolymerization potential on the overoxidation behavior of PEDOT-PPy composite films in aqueous solutions was studied by potentiodynamic method, and the results were shown in Fig. 1. It can be seen that in the first polymerization cycle, the oxidation current of the PEDOT-PPy composite film increased with the increase in the positive potential, whereas at higher potentials (exceeding 1.3 V vs SCE), the oxidation

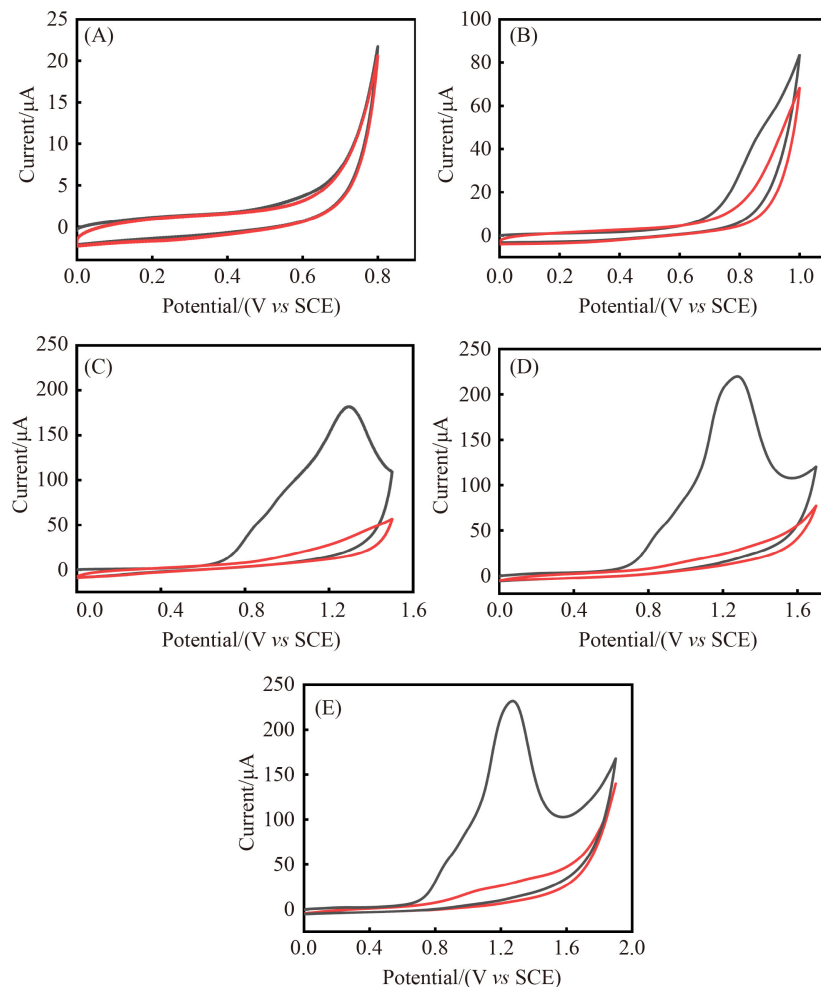


**Fig. 1** CV polymerization curves of PEDOT-PPy/GCE with LiClO<sub>4</sub>-water as the electrolyte at different polymerization potentials. The black and red lines represent the first and second polymerization cycles, respectively. (A) 0–0.8 V; (B) 0–1.0 V; (C) 0–1.5 V; (D) 0–1.7 V; (E) 0–1.9 V.

current decreased rapidly. In the second polymerization cycle, the electropolymerization behavior of PEDOT-PPy prepared in the potential range of 0–0.8 V remained stable. However, when the positive limit of electrode potential was 1.0 V or higher, the oxidation current decreased more obviously, which implied that more oPEDOT-oPPy films were formed on the GCE, causing a decrease in conductivity of composite films [8,26]. This electrochemical overoxidation behavior may be related to that of single PEDOT and PPy film [27,28].

### 3.1.2 DPV analysis

In Fig. 2, DPV method was used to investigate not only the influence of positive potential limit on the electroactivity of PEDOT-PPy/GCE, but also influence of incubation on the electroactivity of single and composite electrode. As shown in Fig. 2(A) and 2(B), the DPV peak current of rutin and luteolin, especially of rutin, on the composite electrode gradually decreased or even disappeared with the increase in the positive potential limit before incubation. This may be attributed to the formation of oPEDOT-oPPy, which was consistent with the CV polymerization results. After incubation, the DPV peak current of rutin and luteolin on the composite electrode prepared in the polymerization range of 0–0.8 and 0–1.0 V

decreased, indicating that the incubation in alkaline condition led to a decrease in the electroactivity of PEDOT-PPy/GCE, which was consistent with the reported literature [14]. However, when the positive limit of the electrode potential was 1.5 V and higher, the DPV peak current of rutin and luteolin on the composite electrode increased obviously. Taking luteolin as an example, the current on the composite electrode prepared at 0–0.8 and 0–1.0 V decreased by nearly 1.9 and 3.6 times, while that on the electrode prepared at 0–1.5, 0–1.7, and 0–1.9 V increased by approximately 1.7, 4.2, and 4.5, respectively. Further, the composite electrode prepared in the potential range of 0–1.7 V after incubation had the largest peak current for rutin and luteolin. Consequently, the incubation in NaOH–ethanol solution can be used as an effective means to improve the electrocatalytic performance of oPEDOT-oPPy composite electrode prepared at high positive limit potentials ( $\geq 1.5$  V).

Under fixed monomer concentration of 6 mmol·L<sup>-1</sup> and polymerization potential range of 0–1.7 V, oPPy/GCE, oPEDOT/GCE, and oPEDOT-oPPy/GCE ( $n_{\text{EDOT}}:n_{\text{Py}} = 2:1$ ) were prepared for rutin and luteolin detection. It can be seen from Fig. 2(C) that the GCE had similar peak currents for both rutin ( $I_{\text{Ru}}$ ) and luteolin ( $I_{\text{Lu}}$ ), where the ratio of  $I_{\text{Lu}}$  to  $I_{\text{Ru}}$  ( $I_{\text{Lu}}/I_{\text{Ru}}$ ) before and after incubation was 1.2 and 1.0, respectively, indicating that the incubation

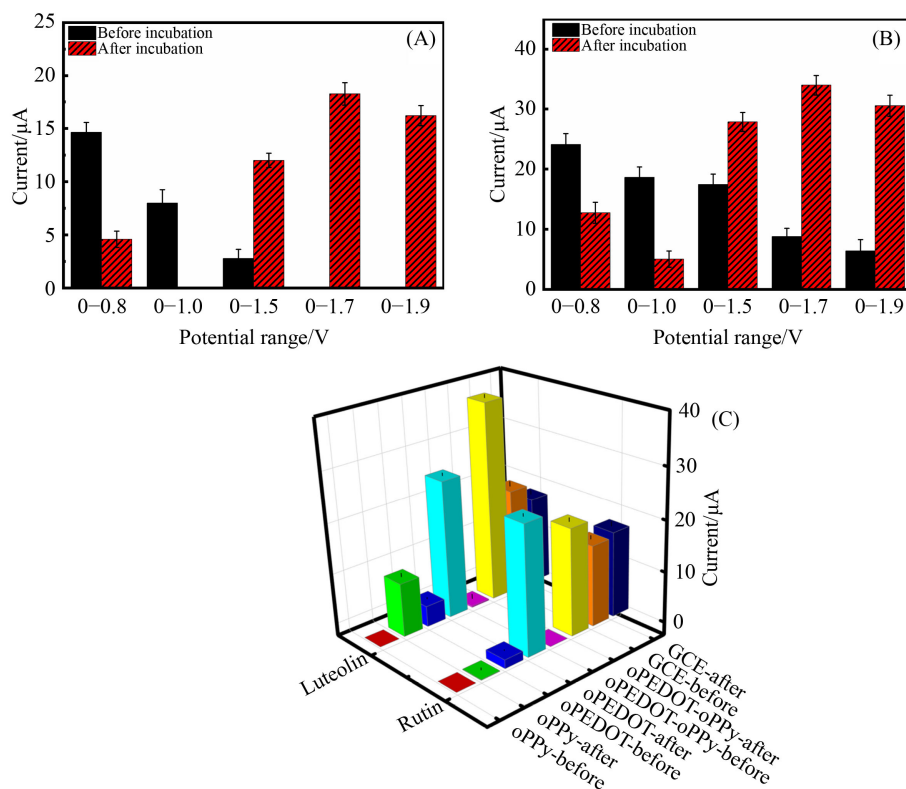


**Fig. 2** Histograms for DPV detection of (A) rutin and (B) luteolin in PEDOT-PPy composite films prepared under different potential ranges before and after incubation; (C) histograms of DPV peak currents measured in 15  $\mu\text{mol}\cdot\text{L}^{-1}$  rutin and luteolin in 0.1  $\text{mol}\cdot\text{L}^{-1}$  ABS (pH 4.2) before and after incubation of various electrode materials. Incubation solvent: NaOH–ethanol solution; incubation time: 30 min.

had a minor effect on the electrocatalytic performance of GCE. oPPy/GCE had the smallest current for rutin and luteolin, but it had the highest  $I_{Lu}/I_{Ru}$  value after incubation (88). This may be due to the permeaselectivity of oPPy which was more suitable for small molecule luteolin to pass through and reach the surface of active electrode [29]. Before incubation, although oPEDOT/GCE had the highest peak current for rutin and luteolin, it was still at a relatively low current level. After incubation, the current on this electrode increased 20-fold for rutin and 6-fold for luteolin, respectively, indicating that incubation was conducive to the improvement of oPEDOT's electrocatalytic activity.

The DPV peak current of rutin and luteolin on oPEDOT-oPPy/GCE was lower than that on oPEDOT/GCE before incubation. After incubation, the  $I_{Ru}$  on the composite electrode significantly increased, which was higher than that on oPPy/GCE but lower than that on oPEDOT/GCE, showing the high electrocatalytic ability of oPEDOT. However, the  $I_{Lu}$  on the composite electrode was higher than that on the single material, and the  $I_{Lu}/I_{Ru}$  of the composite electrode after incubation was 1.9, higher than that of oPEDOT/GCE ( $I_{Lu}/I_{Ru} = 1.1$ ). These results indicated that the presence of oPPy enhanced the selectivity of the composite electrode, thereby further improving the electrocatalytic ability of the composite electrode for luteolin. Therefore, the oPEDOT and oPPy showed synergistic effect to facilitate enhanced electrocatalytic performance of the composite electrode for luteolin.

### 3.1.3 EIS analysis

The electrochemical behavior of the various electrodes was also investigated using EIS. Figure S1 (cf. Electronic Supplementary Material, ESM) depicted the Nyquist plots of the various electrodes recorded in 0.1 mol·L<sup>-1</sup> KCl solution containing 5 mmol·L<sup>-1</sup> [Fe(CN)<sub>6</sub>]<sup>3-/4-</sup>. The semicircle in the high-frequency region was caused by charge transfer resistant ( $R_{ct}$ ) at electrodes-solution interface. The larger the diameter of the semicircle, the larger the  $R_{ct}$ , that is, the larger the charge transfer resistance. A large semicircle in high-frequency region was observed for oPEDOT-oPPy/GCE before incubation ( $R_{ct} = 451.4 \Omega \cdot \text{cm}^2$ ). However, the diameter of the semicircle was significantly reduced after incubation ( $R_{ct} = 49.8 \Omega \cdot \text{cm}^2$ ), indicating the decreased charge transfer resistance of oPEDOT-oPPy/GCE toward probe molecules. The  $R_{ct}$  values of oPEDOT/GCE and oPPy/GCE was 199.5 and 530.8  $\Omega \cdot \text{cm}^2$  before incubation, 18.9  $\Omega \cdot \text{cm}^2$  and 813.6  $\Omega \cdot \text{cm}^2$  after incubation, respectively. Therefore, it can be inferred that the presence of oPEDOT promoted the electroactivity of oPEDOT-oPPy after incubation. As a control, the EIS of PEDOT/GCE and PPy/GCE were investigated. The  $R_{ct}$  values of PEDOT/GCE and PPy/GCE after incubation (61.6 and 26.5  $\Omega \cdot \text{cm}^2$ )

was ~10 and 4 times larger than before incubation (6.5 and 7.1  $\Omega \cdot \text{cm}^2$ ), respectively, which may be due to the increased resistance caused by the overoxidation of the polymer under alkaline conditions. These results further indicated that incubation significantly improved the electrocatalytic ability of oPEDOT-oPPy/GCE, which were consistent with the DPV results.

### 3.1.4 Estimation of effective specific surface area

The effective specific surface area of PEDOT-PPy/GCE prepared under different polymerization potential ranges before and after incubation was estimated by CC method. Based on Anson equation [30], the effective specific surface area can be calculated as follows:

$$Q(t) = \frac{2nFACD^{1/2}t^{1/2}}{\pi^{1/2}} + Q_{dl} + Q_{ads}, \quad (2)$$

where  $Q_{ads}$  is the Faraday charge,  $D$  is the diffusion coefficient of the electrode,  $A$  is the effective specific surface area of the working electrode, and  $n$  is the number of electron transfers. In 1 mmol·L<sup>-1</sup> K<sub>3</sub>[Fe(CN)<sub>6</sub>] solution,  $D = 7.60 \times 10^{-6} \text{ cm}^2 \cdot \text{s}^{-1}$ , and  $n = 1$ .

It can be seen in Fig. S2 (cf. ESM) and Table 1 that the slope of  $Q$  vs.  $t^{1/2}$  curve after incubation was larger than that before incubation. In the potential range of 0–1.5, 0–1.7, and 0–1.9 V, the  $A$  value of the composite electrode after incubation was 2.5, 2.9, and 2.1 times higher than that before incubation, respectively. The increase in  $A$  value of the incubated electrode prepared at high potential limit ( $\geq 1.5$  V) was more significant than that of the electrode prepared at low potential limit (0.8 V, 1.0 V). Further, the composite electrode prepared in the potential range of 0–1.7 V exhibited the most prominent increase in  $A$  value. There was a slight change in  $A$  value of GCE before and after incubation, which was smaller than that of the composite electrode. This meant that the incubation can improve the effective specific surface area of the composite film, especially when it was prepared in the potential range with higher positive limit of electrode potential, thereby enhancing the adsorption ability for rutin and luteolin.

### 3.1.5 Estimation of standard electron transfer rate constant

The electron transfer rate constant between the oPEDOT-oPPy composite electrode after incubation and the responsive molecules can be investigated by CC method. The  $k_s$  value was calculated by the following Velasco's equation [31]:

$$k_s = 2.4 \times \exp\left(-\frac{0.02F}{RT}\right) \times D^{1/2} \times (E_p - E_{p/2})^{-1/2} \times v^{1/2}, \quad (3)$$

where  $E_{p/2}$  is the potential corresponding to the half peak height, and  $v$  is the scanning rate (10 mV·s<sup>-1</sup>).

According to Eq. (2) and Table 1, the  $D$  value can be

determined based on the slope of charge vs  $t^{1/2}$  curve (Fig. S3, cf. ESM). Then, the value of  $k_s$  can be calculated using Eq. (3), and the results were shown in Table 2. The  $k_s$  values of the composite electrode prepared in the potential range of 0–1.5, 0–1.7, and 0–1.9 V for rutin and luteolin were higher than those prepared in other two potential range. Among them, the electrode prepared in the potential range of 0–1.7 V had the highest  $k_s$  value, that is, the fastest electron transfer rate between the electrode and the tested solution, thereby exhibiting the strong electrocatalytic ability for rutin and luteolin.

### 3.2 Optimization of incubation conditions

oPEDOT-oPPy/GCE prepared in the potential range of 0–1.7 V were incubated in NaOH–ethanol solution, 0.1 mol·L<sup>-1</sup> NaOH solution, pH 4.2 ABS, pH 8.0 phosphoric acid buffer, deionized water, and ethanol. The DPV peak current of rutin and luteolin on the composite electrode after incubation was determined to optimize the incubation solution. As shown in Fig. 3, after incubation in acidic, neutral, weakly alkaline, anhydrous ethanol solutions, the DPV current of rutin and luteolin on oPEDOT-oPPy/GCE was smaller than that of incubation in strongly alkaline solution. The peak current after the

**Table 1** Calculated effective specific surface area of PEDOT-PPy/GCE prepared under different potential ranges before and after incubation in 0.1 mol·L<sup>-1</sup> KCl containing 1.0 mmol·L<sup>-1</sup> K<sub>3</sub>[Fe(CN)<sub>6</sub>]

Potential range	Before incubation		After incubation	
	Slope	$A/cm^2$	Slope	$A/cm^2$
0–0.8	6.72	0.0224	12.76	0.0425
0–1.0	10.79	0.0359	14.08	0.0469
0–1.5	9.63	0.0321	24.35	0.0811
0–1.7	7.18	0.0239	20.79	0.0693
0–1.9	11.27	0.0375	24.04	0.0801
GCE	5.96	0.0199	5.78	0.0193

**Table 2** Calculated electron transfer rate constant of PEDOT-PPy/GCE in rutin and luteolin solution with a concentration of 10  $\mu\text{mol}\cdot\text{L}^{-1}$

Potential range		Slope	$D/(cm^2\cdot s^{-1})$	$(E_p - E_{p/2})/mV$	$k_s/(cm\cdot s^{-1})$
0–0.8	Rutin	10.76	0.0135	60	0.0523
	Luteolin	10.10	0.0117	46	0.0555
0–1.0	Rutin	15.94	0.0244	–	–
	Luteolin	6.70	0.0043	113	0.0215
0–1.5	Rutin	26.00	0.0217	43	0.0782
	Luteolin	26.07	0.0218	54	0.0699
0–1.7	Rutin	27.47	0.0331	47	0.0925
	Luteolin	28.80	0.0364	54	0.0904
0–1.9	Rutin	26.55	0.0232	44	0.0799
	Luteolin	27.91	0.0256	55	0.0752

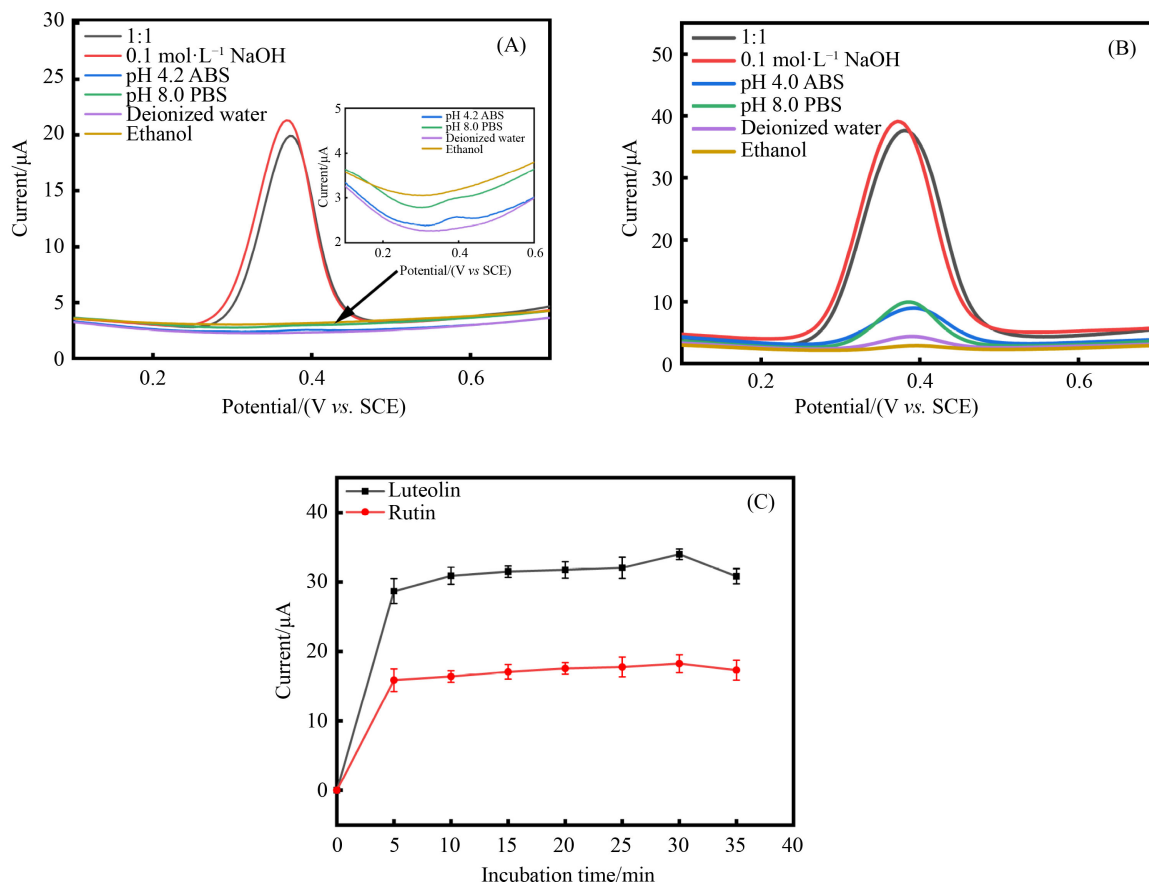


**Fig. 3** DPV measurement of oPEDOT-oPPy/GCE incubated in different solvents for 15  $\mu\text{mol}\cdot\text{L}^{-1}$  (A) rutin and (B) luteolin; (C) DPV peak currents of oPEDOT-oPPy/GCE after different incubation times for 15  $\mu\text{mol}\cdot\text{L}^{-1}$  rutin and luteolin solutions.

electrode incubated in  $0.1 \text{ mol}\cdot\text{L}^{-1}$  NaOH solution was slightly higher than that in NaOH–ethanol solution, but the relative standard deviation value of the former (6.78%,  $n = 3$ ) was larger than that of the latter (1.17%,  $n = 3$ ), indicating that the oPEDOT-oPPy/GCE exhibited poor stability after incubation in NaOH solution. Consequently, NaOH–ethanol solution was selected as the optimum incubation solution.

Before incubation, the composite electrode had little or no current response to the luteolin and rutin. After incubation for 5 min, the peak current on the electrode increased sharply. With the increase in the incubation time, the peak current increased slowly and reached the maximum at 30 min. Therefore, the optimum incubation time was 30 min.

### 3.3 Analytical determination of rutin and luteolin on oPEDOT-oPPy/GCE

The oPEDOT-oPPy/GCE was employed to detect rutin and luteolin in pH 4.2 ABS by DPV methods (the pH effect on DPV current was seen in Section 3.3 and Fig. S4 (cf. ESM)). From Fig. S5 (cf. ESM), it can be seen that the oxidation peak currents increase linearly with the concentrations of rutin and luteolin. For rutin, the corresponding linear equations were  $I = 4.28C + 0.18$  ( $R^2 = 0.998$ ) in the range of  $0.5 \text{ nmol}\cdot\text{L}^{-1}$ – $2.5 \text{ }\mu\text{mol}\cdot\text{L}^{-1}$  and  $I = 0.49C + 11.28$  ( $R^2 = 0.994$ ) in the range of  $4$ – $20 \text{ }\mu\text{mol}\cdot\text{L}^{-1}$ . For luteolin, the corresponding linear equations were  $I = 43.33C + 0.28$  ( $R^2 = 0.997$ ) in the range of  $0.1 \text{ nmol}\cdot\text{L}^{-1}$ – $0.1 \text{ }\mu\text{mol}\cdot\text{L}^{-1}$  and  $I = 2.09C + 5.73$  ( $R^2 = 0.991$ ) in the range of  $1$ – $20 \text{ }\mu\text{mol}\cdot\text{L}^{-1}$ . The limit of detection of rutin and luteolin by oPEDOT-oPPy/GCE measured based on signal to noise ratio at 3 were calculated to be 0.35 and  $0.06 \text{ nmol}\cdot\text{L}^{-1}$ , respectively. A comparison of different modified electrodes for rutin and luteolin analysis was summarized in Table S1 (cf. ESM), which showed that oPEDOT-oPPy/GCE possessed a relative wider detection range and lower detection limit. In addition, it can be seen from Fig. S6 (cf. ESM) that oPEDOT-oPPy/GCE showed good anti-interference ability with a relative error less than 5.0%.

### 3.4 Scanning electron microscopy (SEM) analysis

The SEM images of oPEDOT-oPPy film at different incubation times were shown in Fig. 4. It can be seen in Figs. 4(A) and 4(E) that oPEDOT-oPPy film contained small dispersed particles before incubation. After incubation for 10 min, the particle surface was covered with some lamellar structure (Figs. 4(B) and 4(F)). With the increase of the incubation time, the granular structure disappeared, and long lamellar structures were observed, which were interwoven together to form scattered daylily-like structure (Figs. 4(C) and 4(G)). After incubation for 30 min (Figs. 4(D) and 4(H)), stacked radial tree structure was observed, indicating that the oPEDOT-oPPy film became longer and more orderly with the increase of incubation time, which was beneficial to increase the interaction between polymerization chains [32] and improved the effective specific surface area of the electrode.

### 3.5 Structural analysis

#### 3.5.1 XPS analysis

The XPS spectra of O1s, N1s, and S2p were obtained for the composite film at different incubation times to investigate the overoxidation degree of the oPEDOT-oPPy composite film. It can be seen from Fig. 5 and Table S2 (cf. ESM) that the O1s spectrum of composite films contains four peaks, which corresponded to  $-\text{SO}_2/$   $-\text{SO}$ ,  $-\text{C}=\text{O}/-\text{O}-\text{C}=\text{O}$ ,  $-\text{C}-\text{O}-\text{C}-$ , and  $-\text{COOH}$  [33,34] according to the binding energy from low to high. Except for  $-\text{C}-\text{O}-\text{C}-$ , the other three peaks represented the oxidized groups of the composite film. The  $-\text{C}=\text{O}/-\text{O}-\text{C}=\text{O}$  structure was generated during the electrochemical polymerization process of the composite films, indicating that the film undergone overoxidation reaction due to the nucleophilic attack by  $\text{HO}\cdot$  or dissolved  $\text{O}_2^-$  generated by the electrolysis of water [7,12], while in the thiophene ring, few S atoms were attacked to produce  $-\text{SO}_2/$   $-\text{SO}$  group [8,13]. The content of  $-\text{C}=\text{O}$  group was about a quarter of the total oxygen content, which was much

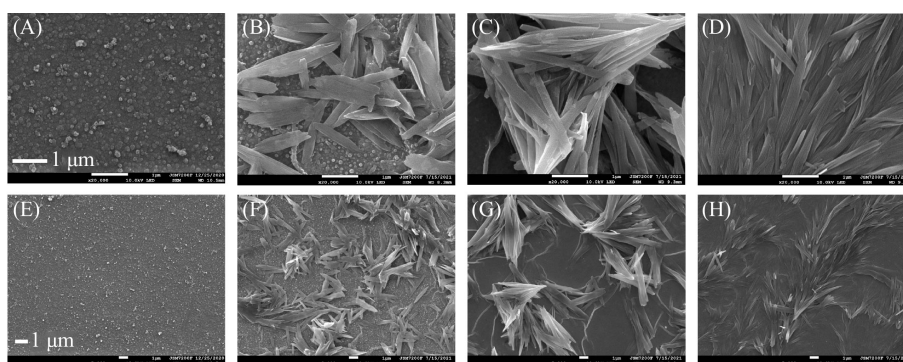


**Fig. 4** SEM images of oPEDOT-oPPy film at low (5 $\times$ ) and high (20 $\times$ ) magnifications under different incubation times: (A, E) 0 min; (B, F) 10 min; (C, G) 20 min; (D, H) 30 min. Incubation solution: NaOH–ethanol solution.

larger than that of the  $-\text{SO}_2/-\text{SO}$  group, indicating that the  $-\text{C}=\text{O}$  group was more easily formed in composite films in the electropolymerization process.

After incubation for 10 min, the content of  $-\text{SO}_2/-\text{SO}$  group in the composite films reached 22.4%, which was about 15 times of that before incubation, but the content of  $-\text{C}=\text{O}$  group showed a slight increase compared with that before incubation, indicating that  $\text{S}^+$  in the thiophene ring was easily overoxidized in the incubation solution. With the increase of incubation time, there was a minor

change in the content of each component, indicating that the overoxidation of oPEDOT-oPPy composite films occurred within 10 min.

As shown in Fig. 6, the N1s spectra can be deconvoluted into four peaks, which corresponded to the  $-\text{C}-\text{N}/-\text{C}=\text{N}-$ ,  $-\text{NH}-$ ,  $-\text{C}-\text{N}^+$  polaron, and  $-\text{C}=\text{N}^+$  bipolaron [35,36]. Table S3 (cf. ESM) showed the contents of N1s components. Before and after incubation, the pyrrole ring in the complex existed mainly in the reduced form ( $-\text{NH}-$ ). After incubation for 10 min, the content of

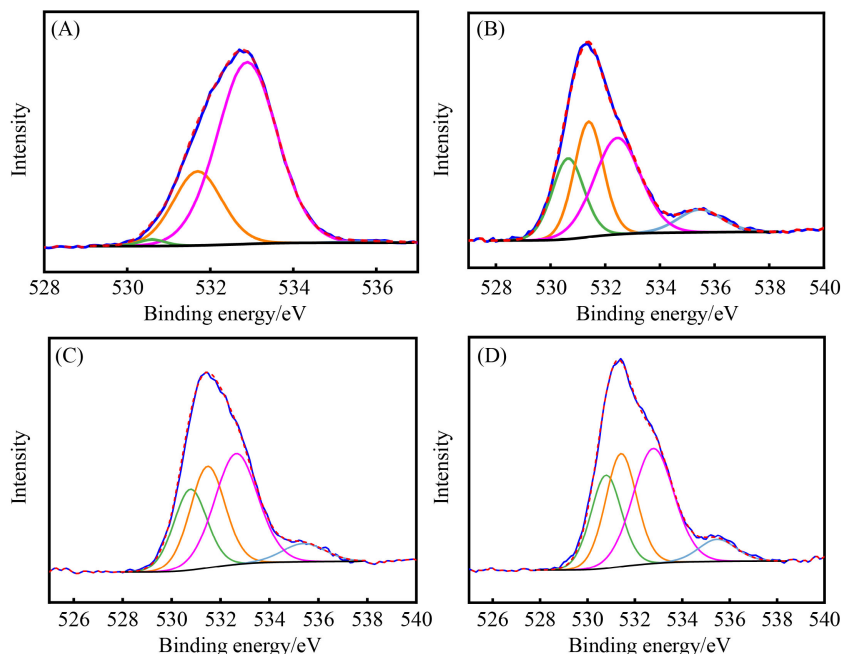


**Fig. 5** XPS O1s spectra of oPEDOT-oPPy films incubated (A) 0 min, (B) 10 min, (C) 20 min and (D) 30 min.

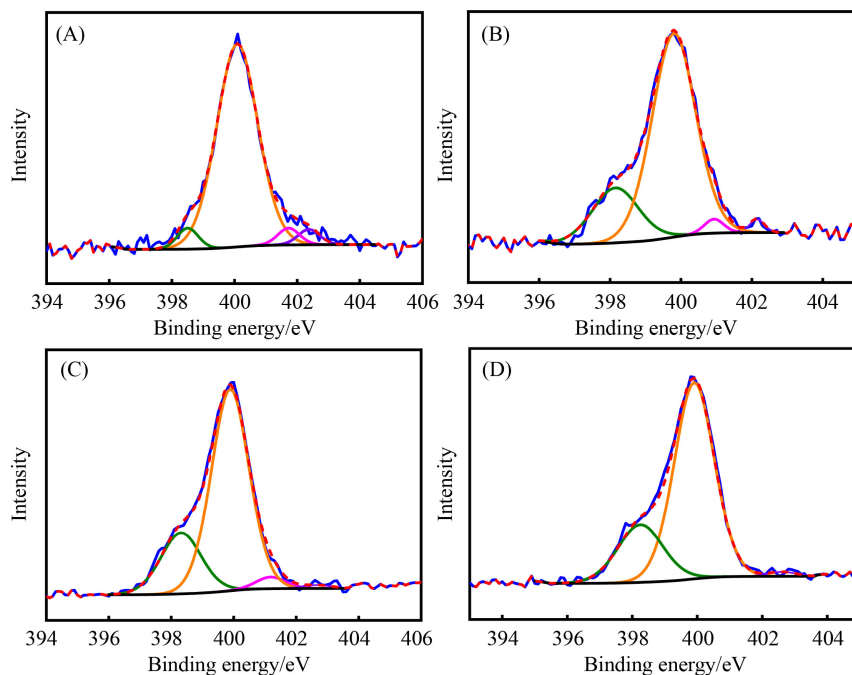


**Fig. 6** XPS N1s spectra of oPEDOT-oPPy films incubated (A) 0 min, (B) 10 min, (C) 20 min and (D) 30 min.

oxidized state  $N^+$  and reduced state  $-NH-$  decreased, while the content of  $-C=N-/C=N-$  increased, indicating that  $ClO_4^-$  can be easily dedoped, and the H atom in  $-NH-$  structure can easily dissociate under alkaline conditions, which promoted the formation of  $-C=N-$  and  $-C_\alpha=C_\beta-$  bond. This may result in a transition of pyrrole ring from benzene type to quinone type [37].

As shown in Fig. 7, the S2p spectra can be deconvoluted into five peaks, which were ascribed to the neutral state ( $S2p_{3/2}$ ,  $S2p_{1/2}$ ), oxidized state ( $S^+$ ), and overoxidized state ( $-SO_2/-SO$ ). The binding energy difference between  $S2p_{3/2}$  and  $S2p_{1/2}$  was nearly 1.2 eV, and the area ratio was 2:1, which was consistent with the reported literature [38,39]. Table S4 (cf. ESM) showed that before incubation, the neutral state S and overoxidized state S of EDOT in the composite film accounted for 72.8% and 21.3%, respectively, indicating that the overoxidation reaction of EDOT occurred at high polymerization potential. After incubation, the content of neutral state S of EDOT decreased to 60.2%, while that of  $-SO_2/-SO$  group increased to 34.8%, suggesting that the oxidized  $S^+$  was susceptible to the attack of  $OH^-$  to generate more  $-SO_2/-SO$  groups.

### 3.5.2 Raman and FTIR spectra

Raman and FTIR spectra were used to investigate the structural changes in the single oPPy, oPEDOT, and oPEDOT-oPPy composite films before and after incubation for 30 min. According to the Raman and FTIR spectra of oPPy and oPEDOT films in Section 3.5.2 (cf.

ESM), after incubation, the adsorption peaks of  $-C=N-$  group was observed. In the pyrrole ring, there existed both benzene-type and quinone-type configurations. By peak fitting, the absorption peak of benzene-type pyrrole ring was more clearly observed in oPPy films compared to quinoid-type pyrrole ring [40]. The structure of thiophene ring changed from benzene-type to quinoid-type (Fig. S7, cf. ESM) in oPEDOT films [32]. These structural changes may result in the enhanced conjugation of single polymers after incubation [32,40,41].

Raman and FTIR were employed to investigate the structural changes of oPEDOT-oPPy composite films before and after incubation in Fig. 8. According to the Raman spectra in Fig. 8(A), before incubation, the absorption peak at  $1571\text{ cm}^{-1}$  was attributed to the  $-C=C-$  bond in the benzene-type pyrrole ring structure [42]. And the peaks at  $1500$  and  $1445\text{ cm}^{-1}$  were assigned to the  $-C_\alpha=C_\beta-$  structure of thiophene ring [43], indicating the successful formation of oPEDOT-oPPy composite film. The absorption peak at  $1445\text{ cm}^{-1}$  shifted to  $1436\text{ cm}^{-1}$ , and the its width decreased, indicating that the structure of thiophene ring in the composite film transformed from benzene-type to quinone-type, which exhibited the enhanced conjugation effect [40,41]. The characteristic peak of pyrrole ring appearing at  $930\text{ cm}^{-1}$  after incubation was ascribed to the  $-C-H-$  out-of-plane deformation vibration caused by the bipolaron ( $-C=N^+-$ ), which further promoted the formation of quinone-type structure [44].

Figure 8(B) showed the FTIR spectra of oPEDOT-oPPy film before and after incubation. New obvious peaks

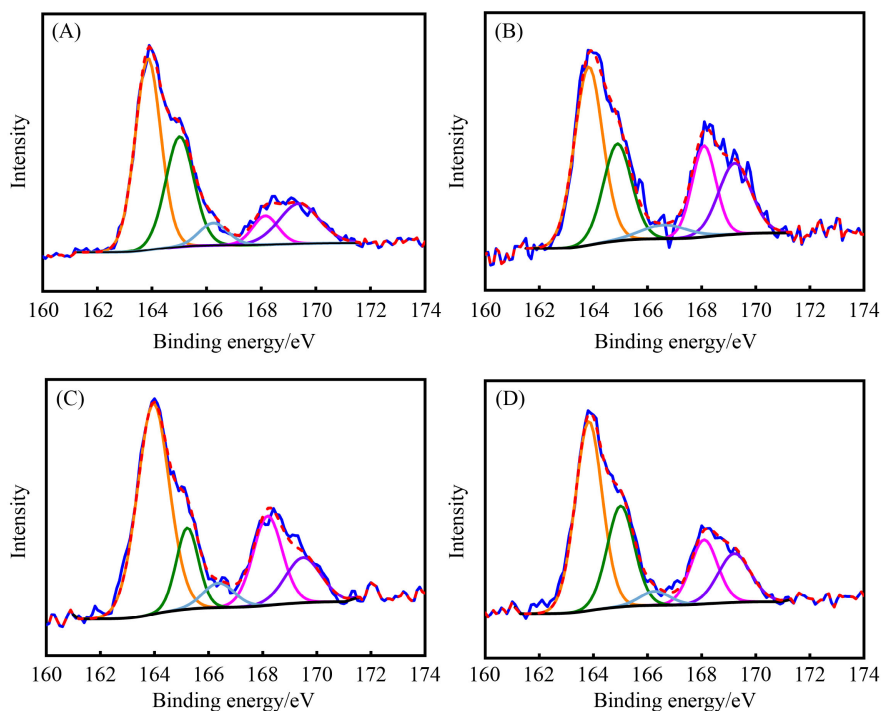


Fig. 7 XPS S2p spectra of oPEDOT-oPPy films incubated (A) 0 min, (B) 10 min, (C) 20 min and (D) 30 min.

appeared at 1633, 1523, and 865  $\text{cm}^{-1}$  after incubation. The peak at 1633  $\text{cm}^{-1}$  was attributed to the generation of  $-\text{C}=\text{N}-$  bond in the pyrrole ring and  $-\text{C}_\alpha=\text{C}_\beta-$  bond in the quinone-type thiophene ring [45]. Also, the peak at 1523  $\text{cm}^{-1}$  was ascribed to the quinoid-type thiophene ring [46]. The absorption peak of  $-\text{SO}_2/-\text{SO}$  group was observed at 1121  $\text{cm}^{-1}$  [47], suggesting the overoxidation of thiophene ring after incubation. Therefore, according to the above results, it can be inferred that incubation promoted the generation of quinoid-type thiophene ring,  $-\text{SO}_2/-\text{SO}$  group, and  $-\text{C}=\text{N}-$  group, which was consistent with XPS results.

### 3.6 Discussion on electrocatalytic mechanism of oPEDOT-oPPy composite films

According to the above analysis, the electrocatalytic ability of the composite film was enhanced after incubation due to the change in its structure. We further explored the underlying mechanism for this improvement. The preparation process of the oPEDOT-oPPy/GCE and the proposed structural change before and after incubation were shown in Fig. 9.

Before incubation, at high potential, due to the nucleophilic attack of  $\cdot\text{OH}$  or dissolved  $\text{O}_2^-$ , the  $-\text{C}=\text{O}$  groups

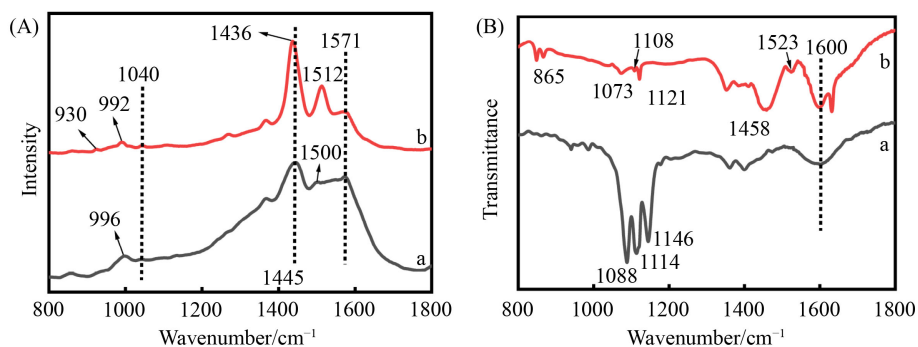


**Fig. 8** (A) Raman spectra under 514 nm laser excitation and (B) FTIR spectra of oPEDOT-oPPy composite films (a) before and (b) after incubation.

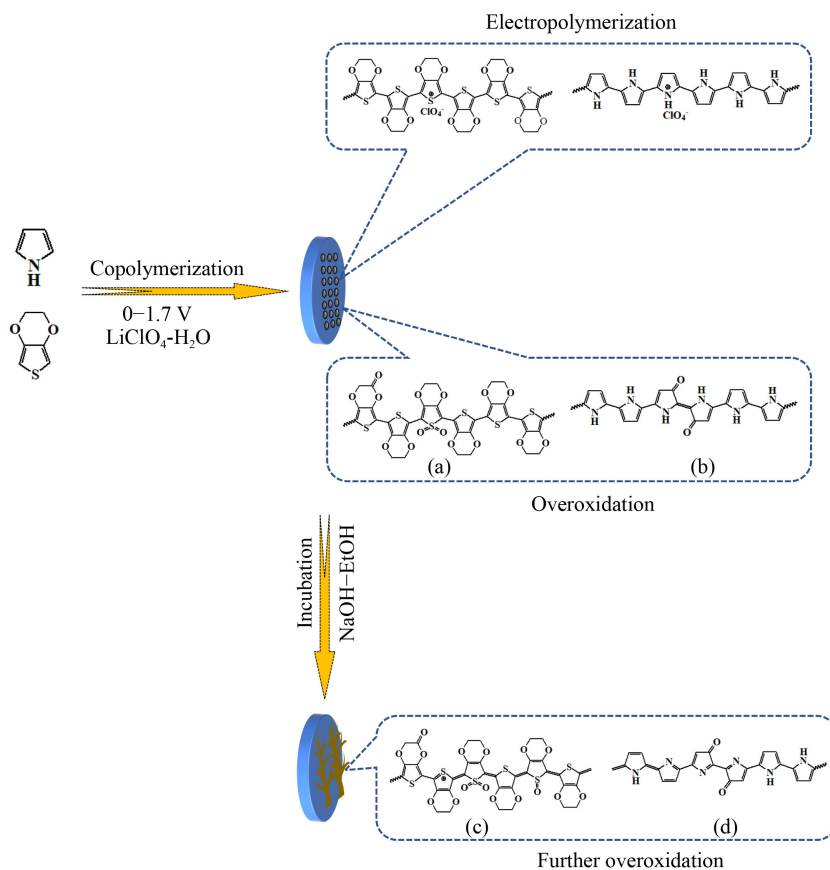


**Fig. 9** Schematic diagram for the preparation process of oPEDOT-oPPy composite films and the proposed structural change before and after incubation.

were generated in the oPEDOT-oPPy composite films at the  $\beta$ -C atom on the pyrrole ring and the saturated C atom on the ethylenedioxy group [7,12], and the  $-\text{SO}_2/-\text{SO}$  groups were generated from S atom in the thiophene ring during electropolymerization process [13,33], due to a decrease in conjugation of polymers, eventually causing a decrease in the electroactivity of oPEDOT-oPPy composite films (Fig. S8, cf. ESM).

After incubation, the content of  $-\text{C}=\text{O}$  group increased slightly, but the content of  $-\text{C}=\text{N}-$  structure increased substantially due to the dissociation of H atom of  $-\text{NH}-$ , which may contribute to the formation of the quinone-type structure in the pyrrole ring [48]. Meanwhile, the S atom on the thiophene ring generated sulfonium ions under the stimulation of  $\text{OH}^-$  and further formed  $-\text{SO}$  group, which promoted the transformation of the thiophene ring from benzene-type to quinoid-type structure. So the conjugation effect between polymeric chains in composite film was possibly improved due to these structural changes (Fig. S9, cf. ESM). In addition, the hydrogen bond reaction occurred between overoxidized groups ( $-\text{C}=\text{O}$  and  $-\text{SO}/-\text{SO}_2$ ) in the oPEDOT-oPPy composite films and the hydroxyl groups in the structure of rutin and luteolin, thus improving the adsorption ability for the responsive molecules, thereby further enhancing the electrocatalytic ability of the composite films.

### 3.7 DFT analysis

To further investigate the effect of the structural change in the oPEDOT-oPPy composite film on their electrochemical performance, the oPEDOT<sub>6</sub> (a, c) and oPPy<sub>6</sub> (b, d) before and after incubation were analyzed by DFT method. The structures of a, b, c, and d molecules deduced from structural analysis were displayed in Fig. 9.

#### 3.7.1 Frontier molecular orbital analysis

It can be seen in Fig. S10 (cf. ESM) that the a-HOMO was localized in the thiophene ring, while the a-LUMO was mainly localized in the overoxidized thiophene ring. After incubation, the c-HOMO was transferred from the inner thiophene ring to the inter-thiophene ring due to the formation of the quinoid structure, and the HOMO and LUMO of c molecule show extended  $\pi$ -orbital conjugation over the entire length of the polymer, which increased the overlap and facilitated the electronic transition [49]. Further, it was observed that the b-HOMO was mainly localized in the benzene-type pyrrole ring, while the d-LUMO was localized in the quinoid-type and overoxidized pyrrole ring. In general, the structural change in the oPEDOT<sub>6</sub> and oPPy<sub>6</sub> after incubation affected the spatial distribution of electrons in the composite film.

Figure 10 revealed that the HOMO and LUMO energies of c and d molecules decreased after incubation,

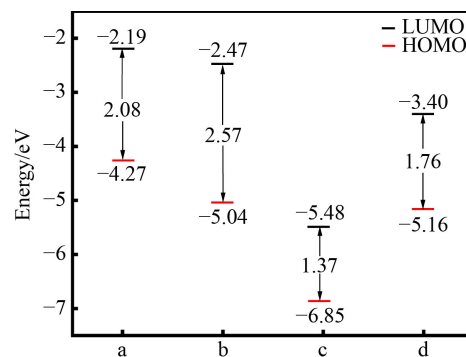


Fig. 10 The frontier molecular orbital energy of (a, c) oPEDOT<sub>6</sub> and (b, d) oPPy<sub>6</sub> before and after incubation.

where c had the lowest energy, i.e., the oPEDOT<sub>6</sub> (c) and oPPy<sub>6</sub> (d) after incubation showed enhanced electron-accepting ability and weak electron-donating ability, so the molecule can be easily reduced. This may be related to the formation of quinoid structures as well as  $-\text{SO}_2/-\text{SO}$  and  $-\text{C}=\text{O}$  electron-withdrawing groups in oPEDOT and oPPy after incubation [50]. Since luteolin was prone to oxidation, it was possible to promote reversible redox reaction between oPEDOT-oPPy and luteolin. The c molecule had the smallest  $E_g$ , followed by the d molecule, indicating that the  $E_g$  of oPEDOT<sub>6</sub> (c) and oPPy<sub>6</sub> (d) became smaller after incubation, which was conducive to the electron transition, thereby enhancing the electrocatalytic ability [46]. In addition, oPEDOT<sub>6</sub>(c) had smallest  $E_g$  value, thus showing strong electrocatalytic ability toward the responsive molecules.

#### 3.7.2 Adsorption energy analysis

Figure S11 (cf. ESM) showed the optimized geometric structure of oPEDOT<sub>6</sub> (a, c) and oPPy<sub>6</sub> (b, d) complexed with luteolin (e) in the oPEDOT-oPPy composite films before and after incubation. According to the front and side views of a/e and c/e, in addition of the two hydrogen bonds formed between the O atom on the sulfone group and the H atom on the o-diphenol hydroxyl group, the H atom on the ethylenedioxy group in the c molecule formed a third hydrogen bond with the  $-\text{C}=\text{O}$  group in the luteolin molecule, indicating enhanced hydrogen bonding interaction between the oPEDOT and luteolin molecules.

According to the front and side views of b/e and d/e complexes, two hydrogen bonds were formed in these complexes, but the length of hydrogen bond in the d/e complex was shorter, indicating a stronger hydrogen bond interaction in the d/e complex. In the optimized geometric structure of the c/e and d/e complexes, the quinoid type five-membered ring structure in the c and d polymers were parallel to the benzene ring structure in the e molecule, which was beneficial to the  $\pi$  electron overlap between the five-membered ring of the c, d structure and the benzene ring of the luteolin (e) molecule, and to enhance adsorption ability of oPEDOT<sub>6</sub> and oPPy<sub>6</sub> for

luteolin.

Furthermore, the calculated adsorption energies  $\Delta E_{ad}$  of oPEDOT<sub>6</sub> (a, c) and oPPy<sub>6</sub> (b, d) for luteolin were listed in Table 3. The  $\Delta E_{ad}$  values of the complexes decreased in the following order: a/e > b/e > d/e > c/e, indicating that the c/e and d/e complexes had more stable structures, and the c and d molecules had a stronger adsorption ability for the e molecule [25]. Therefore, it was inferred that the structural change in the oPEDOT-oPPy composite films after incubation enhanced the electron transition ability of the composite films as well as adsorption ability for luteolin, thereby improving the electrocatalytic performance of the composite films, which further verified the proposed electrochemical mechanism of oPEDOT-oPPy composite films.

## 4 Conclusions

The electrocatalytic ability of oPEDOT-oPPy/GCE for rutin and luteolin was improved significantly after incubation in NaOH–ethanol solution with a volume ratio of 1:1. The oPEDOT-oPPy/GCE prepared in the potential range of 0–1.7 V exhibited larger DPV peak current for luteolin compared with oPEDOT/GCE and oPPy/GCE, which may be due to the strong electrocatalytic ability of oPEDOT and permeaselectivity of oPPy. According to structural analysis, the formation of quinoid structure,  $-\text{SO}_2-\text{SO}$ , and  $-\text{C}=\text{N}-$  groups in the oPEDOT-oPPy composite films promoted the transition of  $\pi$  electrons on the polymer chain and enhanced the adsorption ability for the responsive molecules, thereby improving the electrocatalytic performance. These results were further verified by DFT results. Overall, this work provided an effective solution to circumvent the reduction in the electrocatalytic ability caused by the overoxidation of PEDOT and PPy electrode materials in practical applications.

**Acknowledgements** We greatly appreciate the support of the Key Research and Development (R&D) Projects of Shanxi Province (Grant No. 201903D121114). This project is also supported by Scientific and Technological Innovation Programs of Higher Education Institutions in Shanxi (Grant No. 2020L0667).

**Electronic Supplementary Material** Supplementary material is available in the online version of this article at <https://dx.doi.org/10.1007/s11705-022-2262-z> and is accessible for authorized users.

**Table 3** Adsorption energies for luteolin adsorbed on oPEDOT<sub>6</sub> (a, c) and oPPy<sub>6</sub> (b, d) before and after incubation

Molecule	$E(\text{Hartree})$	Complex	$E_{\text{complex}}(\text{Hartree})$	$\Delta E_{ad}(\text{kcal}\cdot\text{mol}^{-1})$
a	-4979.16	a/e	-6007.23	-28.4
b	-1481.58	b/e	-2509.67	-31.7
c	-5053.45	c/e	-6081.54	-42.5
d	-1479.08	d/e	-2507.16	-32.9
e	-1028.03	–	–	–

## References

- Ye S H, Li G R. Polypyrrole@NiCo hybrid nanotube arrays as high performance electrocatalyst for hydrogen evolution reaction in alkaline solution. *Frontiers of Chemical Science and Engineering*, 2018, 12(3): 473–480
- Zhu H, Li M, Wang D H, Zhou S B, Peng C. Interfacial synthesis of free-standing asymmetrical PPy-PEDOT copolymer film with 3D network structure for supercapacitors. *Journal of the Electrochemical Society*, 2017, 164(9): A1820–A1825
- Wang W, Lv H J, Du J, Chen A B. Fabrication of N-doped carbon nanobelts from a polypyrrole tube by confined pyrolysis for supercapacitors. *Frontiers of Chemical Science and Engineering*, 2021, 15(5): 1312–1321
- Zhao H P, Liu L, Fang Y G, Vellacheri R, Lei Y. Nickel nanopore arrays as promising current collectors for constructing solid-state supercapacitors with ultrahigh rate performance. *Frontiers of Chemical Science and Engineering*, 2018, 12(3): 339–345
- Astratine L, Magner E, Cassidy J, Betts A. Electrodeposition and characterisation of copolymers based on pyrrole and 3,4-ethylenedioxythiophene in BMIM BF<sub>4</sub> using a microcell configuration. *Electrochimica Acta*, 2014, 115: 440–448
- Zainudeen U L, Careem M A, Skaarup S. PEDOT and PPy conducting polymer bilayer and trilayer actuators. *Sensors and Actuators B: Chemical*, 2008, 134(2): 467–470
- Li Y F, Qian R Y. Electrochemical overoxidation of conducting polypyrrole nitrate film in aqueous solutions. *Electrochimica Acta*, 2000, 45(11): 1727–1731
- Wang D T, Pillier F, Cachet H, Debieume-Chouvy C. One-pot electrosynthesis of ultrathin overoxidized poly(3,4-ethylenedioxythiophene) films. *Electrochimica Acta*, 2022, 401: 139472–139480
- Bull R A, Fan F R F, Bard A J. Polymer films on electrodes: VII. Electrochemical behavior at polypyrrole-coated platinum and tantalum electrodes. *Journal of the Electrochemical Society*, 1982, 129(5): 1009–1015
- Du X, Wang Z. Effects of polymerization potential on the properties of electrosynthesized PEDOT films. *Electrochimica Acta*, 2003, 48(12): 1713–1717
- Debieume-Chouvy C, Tran T T M. An insight into the overoxidation of polypyrrole materials. *Electrochemistry Communications*, 2008, 10(6): 947–950
- Lin J M, Su Y L, Chang W T, Su W Y, Cheng S H. Strong adsorption characteristics of a novel overoxidized poly(3,4-ethylenedioxythiophene) film and application for dopamine sensing. *Electrochimica Acta*, 2014, 149: 65–75
- Amanchukwu C V, Gauthier M, Batcho T P, Symister C, Shao-Horn Y, D'Arcy J M, Hammond P T. Evaluation and stability of PEDOT polymer electrodes for Li-O<sub>2</sub> Batteries. *Journal of Physical Chemistry Letters*, 2016, 7(19): 3770–3775
- Gao Z Q, Zi M X, Chen B S. The influence of overoxidation treatment on the permeability of polypyrrole films. *Journal of Electroanalytical Chemistry*, 1994, 373(1-2): 141–148
- Peairs M J, Ross A E, Venton B J. Comparison of nafion- and overoxidized polypyrrole-carbon nanotube electrodes for

- neurotransmitter detection. *Analytical Methods*, 2011, 3(10): 2379–2385
16. Ozcan A, Ilkbas S. Preparation of poly(3,4-ethylenedioxythiophene) nanofibers modified pencil graphite electrode and investigation of over-oxidation conditions for the selective and sensitive determination of uric acid in body fluids. *Analytica Chimica Acta*, 2015, 891: 312–320
  17. Ujvari M, Láng G G, Vesztergom S, Szekeres K J, Kovács N, Gubicza J. Structural changes during the overoxidation of electrochemically deposited poly(3,4-ethylenedioxythiophene) films. *Journal of Electrochemical Science and Engineering*, 2016, 6(1): 77–89
  18. Hui Y, Bian C, Wang J, Tong J, Xia S. Comparison of two types of overoxidized PEDOT films and their application in sensor fabrication. *Sensors*, 2017, 17(3): 628–638
  19. Shetti N P, Mishra A, Basu S, Mascarenhas R J, Kakarla R R, Aminabhavi T M. Skin-patchable electrodes for biosensor applications: a review. *ACS Biomaterials Science & Engineering*, 2020, 6(4): 1823–1835
  20. Ganeshpurkar A, Saluja A K. The pharmacological potential of rutin. *Saudi Pharmaceutical Journal*, 2017, 25(2): 149–164
  21. Gao F, Tu X L, Ma X, Xie Y, Zou J, Huang X G, Qu F L, Yu Y F, Lu L M. NiO@Ni-MOF nanoarrays modified Ti mesh as ultrasensitive electrochemical sensing platform for luteolin detection. *Talanta*, 2020, 215: 120891–120898
  22. Meng R Q, Li Q L, Zhang S J, Tang J K, Ma C L, Jin R Y. GQDs/PEDOT bilayer films modified electrode as a novel electrochemical sensing platform for rutin detection. *International Journal of Electrochemical Science*, 2019, 14(12): 11000–11011
  23. Kulkarni D R, Malode S J, Keerthi Prabhu K, Ayachit N H, Kulkarni R M, Shetti N P. Development of a novel nanosensor using Ca-doped ZnO for antihistamine drug. *Materials Chemistry and Physics*, 2020, 246: 122791–122799
  24. Nespurek S, Kubersky P, Polansky R, Trchova M, Sebera J, Sychrovsky V. Raman spectroscopy and DFT calculations of PEDOT:PSS in a dipolar field. *Physical Chemistry Chemical Physics*, 2021, 24(1): 541–550
  25. Zhang J H, She Y B. Mechanism of methanol decomposition on the Pd/WC(0001) surface unveiled by first-principles calculations. *Frontiers of Chemical Science and Engineering*, 2020, 14(6): 1052–1064
  26. Láng G G, Ujvári M, Vesztergom S, Kondratiev V, Gubicza J, Szekeres K J. The electrochemical degradation of poly(3,4-ethylenedioxythiophene) films electrodeposited from aqueous solutions. *Zeitschrift für Physikalische Chemie*, 2016, 230(9): 1281–1302
  27. Ujvári M, Gubicza J, Kondratiev V, Szekeres K J, Láng G G. Morphological changes in electrochemically deposited poly(3,4-ethylenedioxythiophene) films during overoxidation. *Journal of Solid State Electrochemistry*, 2015, 19(4): 1247–1252
  28. Debiemme-Chouvy C. One-step electrochemical synthesis of a very thin overoxidized polypyrrole film. *Electrochemical and Solid-State Letters*, 2007, 10(12): E24–E26
  29. Farrington A M, Slater J M. Prediction and characterization of the charge/size exclusion properties of over-oxidized poly(pyrrole) films. *Electroanalysis*, 1997, 9(11): 843–847
  30. Anson F C. Application of potentiostatic current integration to the study of the adsorption of cobalt(III)-(ethylenedinitrilo) tetracetate on mercury electrodes. *Analytical Chemistry*, 1964, 36(4): 932–934
  31. Velasco J G. Determination of standard rate constants for electrochemical irreversible processes from linear sweep voltammograms. *Electroanalysis*, 1997, 9(11): 880–882
  32. Ouyang J Y, Xu Q F, Chu C W, Yang Y, Li G, Shinar J. On the mechanism of conductivity enhancement in poly(3,4-ethylenedioxythiophene):poly(styrene sulfonate) film through solvent treatment. *Polymer*, 2004, 45(25): 8443–8450
  33. Marciniak S, Crispin X, Uvdal K, Trzcinski M, Birgeron J, Groenendaal L, Louwet F, Salaneck W R. Light induced damage in poly(3,4-ethylenedioxythiophene) and its derivatives studied by photoelectron spectroscopy. *Synthetic Metals*, 2004, 141(1-2): 67–73
  34. Lan M H, Zhang J F, Chui Y S, Wang H, Yang Q D, Zhu X Y, Wei H X, Liu W M, Ge J H, Wang P F, Chen X, Lee C S, Zhang W. A recyclable carbon nanoparticle-based fluorescent probe for highly selective and sensitive detection of mercapto biomolecules. *Journal of Materials Chemistry B: Materials for Biology and Medicine*, 2015, 3(1): 127–134
  35. Qiao Y S, Shen L Z, Wu M X, Guo Y, Meng S M. A novel chemical synthesis of bowl-shaped polypyrrole particles. *Materials Letters*, 2014, 126: 185–188
  36. Zhang J T, Zhao X S. Conducting polymers directly coated on reduced graphene oxide sheets as high-performance supercapacitor electrodes. *Journal of Physical Chemistry C*, 2012, 116(9): 5420–5426
  37. Wen P, Tan C H, Zhang J C, Meng F B, Jiang L, Sun Y H, Chen X D. Chemically tunable photoresponse of ultrathin polypyrrole. *Nanoscale*, 2017, 9(23): 7760–7764
  38. Ivanko I, Svoboda J, Lukešová M, Šeděnková I, Tomšík E. Hydrogen bonding as a tool to control chain structure of PEDOT: electrochemical synthesis in the presence of different electrolytes. *Macromolecules*, 2020, 53(7): 2464–2473
  39. Blacha A, Koscielniak P, Sitarz M, Szuber J, Zak J. Pedot brushes electrochemically synthesized on thienyl-modified glassy carbon surfaces. *Electrochimica Acta*, 2012, 62: 441–446
  40. Kulandaivalu S, Zainal Z, Sulaiman Y. Influence of monomer concentration on the morphologies and electrochemical properties of PEDOT, PANI, and PPy prepared from aqueous solution. *International Journal of Polymer Science*, 2016, 2016: 1–12
  41. Culebras M, Gómez C M, Cantarero A. Enhanced thermoelectric performance of PEDOT with different counter-ions optimized by chemical reduction. *Journal of Materials Chemistry A: Materials for Energy and Sustainability*, 2014, 2(26): 10109–10115
  42. Chen F E, Shi G Q, Fu M X, Qu L T, Hong X Y. Raman spectroscopic evidence of thickness dependence of the doping level of electrochemically deposited polypyrrole film. *Synthetic Metals*, 2003, 132(2): 125–132
  43. Rodriguez-Jimenez S, Bennington M S, Akbarinejad A, Tay E J, Chan E W C, Wan Z, Abudayyeh A M, Baek P, Feltham H L C, Barker D, Gordon K C, Travas-Sejdic J, Brooker S. Electroactive metal complexes covalently attached to conductive PEDOT films: a spectroelectrochemical study. *ACS Applied Materials &*

- Interfaces, 2021, 13(1): 1301–1313
44. Santos M J L, Brolo A G, Girotto E M. Study of polaron and bipolaron states in polypyrrole by *in situ* Raman spectroelectrochemistry. *Electrochimica Acta*, 2007, 52(20): 6141–6145
  45. Mathys G I, Truong V T. Spectroscopic study of thermo-oxidative degradation of polypyrrole powder by FT-IR. *Synthetic Metals*, 1997, 89(2): 103–109
  46. Song J C, Noh H J, Lee J H, Nah I W, Cho W I, Kim H T. *In situ* coating of poly(3,4-ethylenedioxythiophene) on sulfur cathode for high performance lithium-sulfur batteries. *Journal of Power Sources*, 2016, 332: 72–78
  47. Han Y Q, Shen M X, Wu Y, Zhu J J, Ding B, Tong H, Zhang X G. Preparation and electrochemical performances of PEDOT/sulfonic acid-functionalized graphene composite hydrogel. *Synthetic Metals*, 2013, 172: 21–27
  48. Xie H, Yan M M, Jiang Z Y. Transition of polypyrrole from electroactive to electroinactive state investigated by use of *in situ* FTIR spectroscopy. *Electrochimica Acta*, 1997, 42(15): 2361–2367
  49. Coleone A P, Lascane L G, Batagin-Neto A. Polypyrrole derivatives for optoelectronic applications: a DFT study on the influence of side groups. *Physical Chemistry Chemical Physics*, 2019, 21(32): 17729–17739
  50. Wasim F, Kosar N, Mahmood T, Ayub K. Sensor applications of polypyrrole for oxynitrogen analytes: a DFT study. *Journal of Molecular Modeling*, 2018, 24(11): 308–322